SLAC – PUB – 3772
September 1985
(I)

DEVELOPMENT OF THE ČERENKOV RING IMAGING DETECTOR FOR THE SLD*

V. Ashford, T. Bienz, F. Bird, G. Hallewell, D. Leith, D. McShurley, A. Nuttall,
B. Ratcliff, R. Reif, D. Schultz, S. Shapiro, T. Shimomura,† N. Toge, S. Williams‡
Stanford Linear Accelerator Center, Stanford University, Stanford, California 94306

D. Bauer, D. Caldwell, A. Lu, S. Yellin
University of California, Santa Barbara, CA 93106

M. Cavalli-Sforza, D. Coyne
University of California, Santa Cruz, CA 95064

R. Johnson, B. Meadows, M. Nussbaum
University of Cincinnati, Cincinnati, Ohio 45221

ABSTRACT

Results of recent beam tests of a physics prototype Čerenkov Ring Imaging Detector (CRID) for the SLD are reported. The system includes both liquid (C_6F_{14}) and gas (isobutane) radiators and an 80 *cm* quartz TPC with a gaseous TMAE photocathode and proportional wire readout. Measurements of the quality factor (N_0) and Čerenkov angles of both radiators at various TMAE concentrations and beam momenta are presented. Other system characteristics, including electron lifetimes, spatial resolution, "photon feedback" and preliminary results from third coordinate charge division readout are discussed.

INTRODUCTION

This paper describes recent results from the on-going research and development work on the Čerenkov Ring Imaging Detector (CRID)[1,2] for the SLD.[3] The SLD is a second generation detector for the SLAC Linear Collider (SLC) incorporating several state-of-the-art detectors, and with uniform response over nearly 4 π steradians. It is designed to study Z^0 decays in great detail. The combination of precise secondary vertex detection in the CCD array and the excellent particle identification in the CRID makes a powerful "flavor" tagging system that can suppress combinatorial backgrounds and give a greatly enhanced heavy particle signal. Figure 1 is a quarter section of the SLD showing the relationship of the major components. The CRID uses both liquid and gas radiators to give excellent hadron separation over most of the momentum range of interest at the SLC and helps with the e/π separation below 4 GeV/c where the calorimetry begins to fail. The CRID photon detectors cover 29 m^2 with 1 mm^3 space point resolution on individual Čerenkov photons using photosensitive long drift (75 *cm* maximum) time projection chambers (TPCs) with charge division proportional wire readout. Figure 2 is a CRID quarter section showing the relationship of the liquid and gas radiators, TPC, and mirrors in both the barrel and endcap sections.

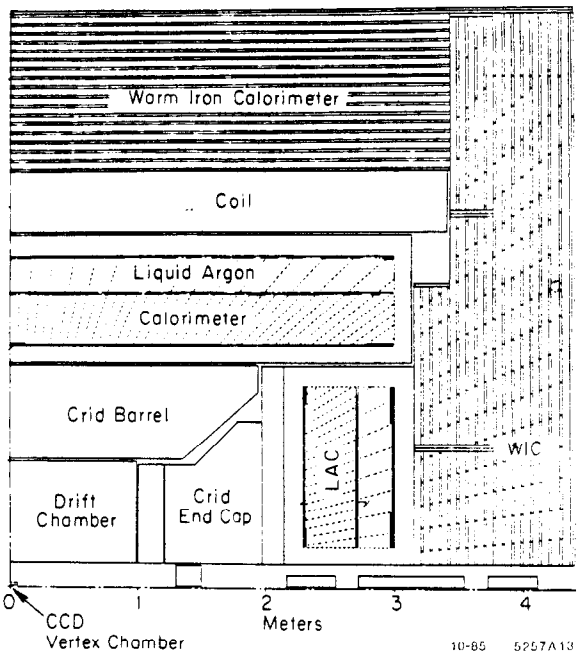

Fig. 1. One quarter cross section of the SLD

PRINCIPLE OF THE CRID

The application of photosensitive gas amplification counters to the detection of individual photons on a focused Čerenkov ring was developed by J. Seguinot and T. Ypsilantis.[4] They envisioned the use of agents such as acetone or triethylamine (TEA) which photoionize below 1600 Å. The discovery by D. Anderson[5] that Tetrakis (Dimethyl Amino) Ethylene (TMAE) could be used as a photocathode in a proportional chamber opened the way for the development of large area ($\sim m^2$) photosensitive detectors. TMAE's low ionization potential (5.36 eV) allows the use of UV quartz windows, making such devices economically feasible. The quartz UV transmission cut off at just below 1700 Å and the TMAE photoionization threshold at about 2300 Å define an operational window of high quantum efficiency as shown in Fig. 3.

* Work supported by the Department of Energy, contract DE-AC03-76SF00515.
† Present Address: 2-80 Miya-cho, Omiya, Saitama, Japan.
‡ Present Address: Diasonics Corp., 533 Cabot St., S. San Francisco, CA 94080

Presented at the Nuclear Science Symposium, San Francisco, California, October 23-25, 1985

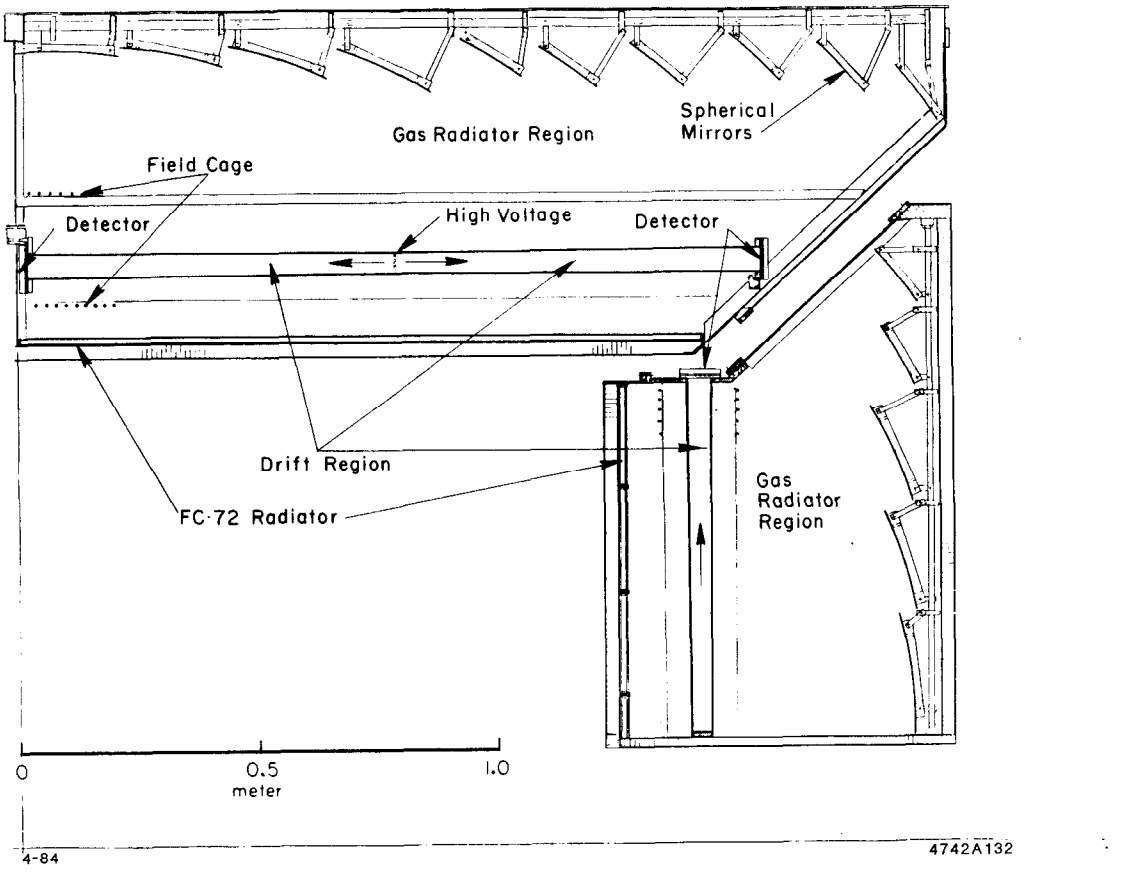

Fig. 2. One quarter section of CRID Barrel and Endcap.

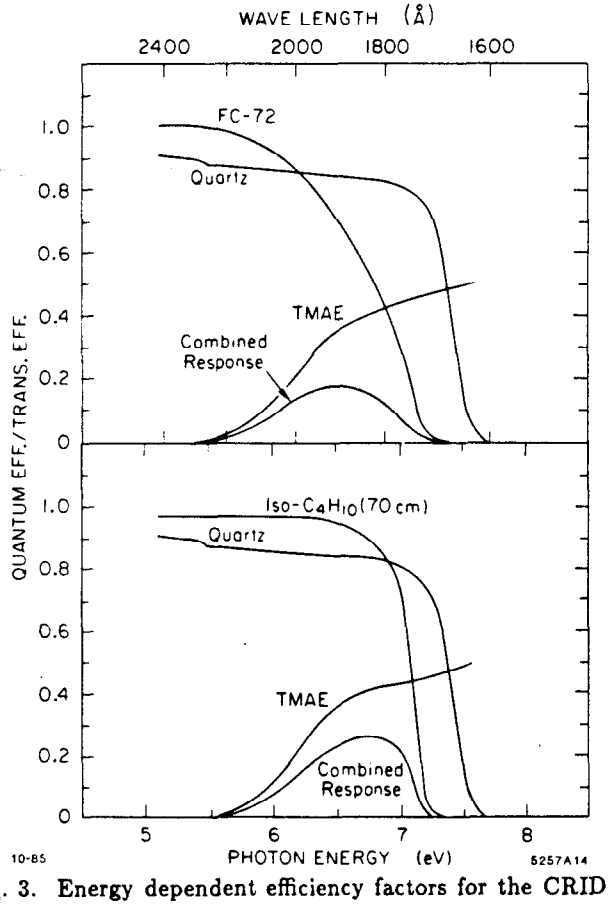

Fig. 3. Energy dependent efficiency factors for the CRID a) liquid radiator and b) gas radiator.

The total number of detected photoelectrons for a Čerenkov counter is given by

$$N_{pe} = \frac{\alpha L}{\hbar c} \int \epsilon(E) \sin^2 \theta_c(E) dE$$

where $\theta_c(E)$ is the Čerenkov angle, L is the radiator length in cm, E is energy in eV and ϵ(E) is the overall efficiency function of the system including such factors as the TMAE quantum efficiency; the transmission and reflection of windows, mirrors, gas or liquid radiator; electron transport and detection efficiency; etc. Taking the weighted average Čerenkov angle out and integrating gives

$$N_{pe} = N_0 L \sin^2 \bar{\theta}_c$$

where N_0 is the conventional figure of merit for a Čerenkov counter expressed per unit radiator length. Figure 3 shows the various factors for the SLD CRID from which N_0 values of $60/cm$ and $90/cm$, corresponding to 23 and 14 photoelectrons, are derived for the liquid and gas radiators respectively.

THE APPARATUS

The apparatus used in these studies is a full scale test cell designed to demonstrate the physics principles of the SLD CRID design. This system, shown in Fig. 4, incorporates the essential features of the SLD CRID including elevated temperature (40°C) to allow heated TMAE mixing (to achieve the desired concentration), both liquid and gas radiators, and a full length photosensitive TPC with proportional wire readout. The apparatus is enclosed in an insulated aluminum vessel which is temperature regulated to better than 1°C and usually

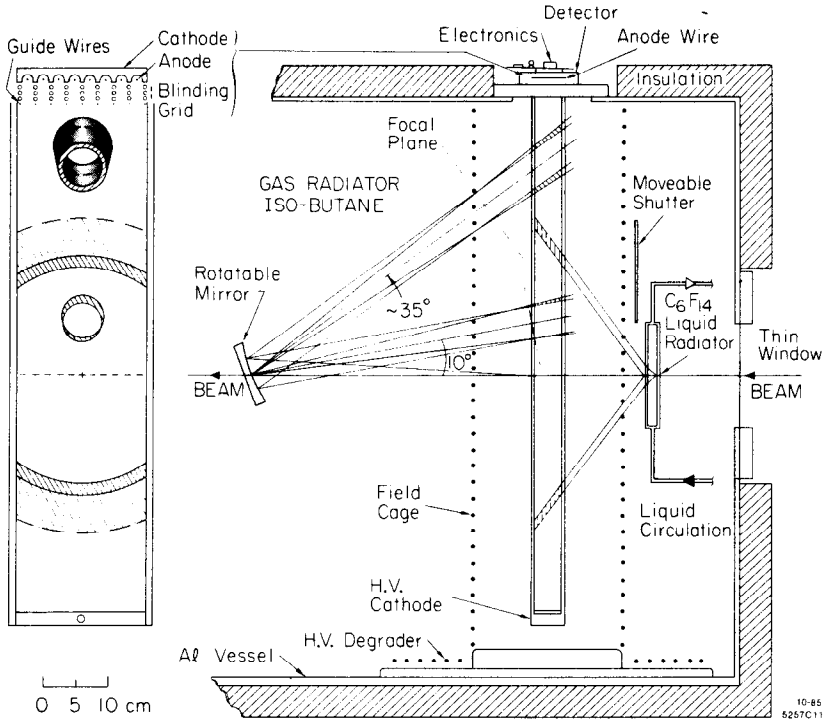

Fig. 4 Schematic of the long drift apparatus showing on the left a transverse view and on the right an elevation of the TPC. Trajectories of photons produced in the liquid and gas radiators are superimposed showing the expected images in the transverse view.

operated at 35°C. This vessel also serves as the container for the gas radiator.

The gas radiator used in these tests was isobutane (C_4H_{10}).[6] It is transparent down to 1700 Å and has a high refractive index of about 1.0017. A small (11 *cm* dia., f4, fl = 44.5 *cm*) telescope mirror placed 43 *cm* from the drift box images the gas ring in the TPC. The mirror was aluminized and coated with MgF_2; its reflectivity at 1700 Å was measured to be 86%.[7] The mirror can pivot about a horizontal axis perpendicular to the beam so that the image can be moved up and down the box, or directed away at will. Note, however, that unlike the SLD design, the image becomes progressively defocused as it is moved away from the beam line, as shown schematically in Fig. 4. In addition the image, without the depth coordinate, becomes severely "parallax" broadened.

The liquid radiator material is perfluorohexane, C_6F_{14}.[6] It is transparent down to 1800 Å and has an average index of refraction of 1.275 between 1800 and 2300 Å. It is contained in a 13 *cm* dia. by 1.27 *cm* thick quartz cell and is continuously circulated through Oxisorb[8] filters to remove oxygen, water and other contaminants that reduce the UV clarity. The transparency is periodically measured in a UV monochromator. A typical curve is shown in Fig. 3a. The Čerenkov radiation from the liquid radiator is "proximity focused" by allowing a drift space between the radiator and the TPC so that the radius r of the annulus of light (with thickness $dr = d\tan\theta_c$, where d is the radiator thickness) can expand to the point where dr/r is acceptable. However, the steep angle ($\sim 53°$ for $\beta = 1$ particle at normal incidence) due to refraction results in substantial "parallax" broadening that is removed by the "third coordinate" measurement.

The TPC box has 80 *cm* by 20 *cm* by 0.32 *cm* Suprasil II[9] quartz windows[10] on each side. It is 4 *cm* thick at the bottom and tapers to 4.8 *cm* at the top; this taper allows electrons produced close to the surface to drift away from the window, thus reducing diffusion losses close to the surface. Both sides of the windows are covered by a fine wire (76 μm) array of field defining electrodes on a 0.254 *cm* pitch. The side walls are "G-10" with Cu traces on both sides. In addition, there is a heavier wire "field cage" on a 2.54 *cm* pitch surrounding the drift box. These electrodes are all linearly graded in potential from the most negative (−50 kV) at the bottom up to the detector potential at the top.

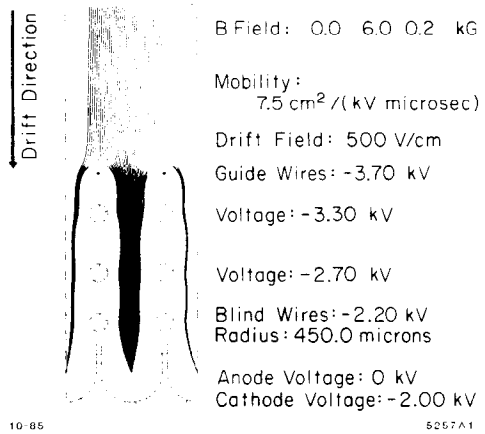

Fig. 5. Electrostatic simulation of the detector electron collection efficiency with a four layer "blinding grid." A 6 kG axial field and a 0.2 kG "radial" field are assumed; the data were taken without field.

The anode wires are 5.5 *cm* long with a 3.175 *mm* pitch. Most of the data were taken with an anode plane of 20 μm dia. gold plated tungsten wires. A small amount of data were taken using an anode plane made of 7 μm dia. carbon fibers, to study "third coordinate" readout by charge division. The resistance of these fibers is about 5 $k\Omega/cm$. Bench tests[11] show that it is possible to achieve better than 2% position resolution on single electron signals at a total charge gain of 2×10^5. The cathode is a machined and nickel plated aluminum block (Fig. 5) with 0.25 *mm* walls between the anode wires to suppress UV photons produced in the charge amplification avalanches ("photon feedback"). The anode to cathode spacing is 1.47 *mm*, and the wall between the anode wires extends $\sim$ 1.5 *mm* above the anode plane. Above this structure there are three planes of 0.9 *mm* dia. wires and one plane of 0.076 *mm* "guide" wires. This "blinding grid" further optically isolates each cell. Each layer of the grid is graded in voltage to focus the incoming electrons onto the anode. The field inside this structure is about four times the drift field. An electrostatic simulation of one detector cell is shown in Fig. 5. Although the data discussed here were taken without a magnetic field, the simulation was done with 6 kG parallel and 0.2 kG transverse magnetic field components to simulate SLD conditions. Some data were taken with the blinding grid removed to study its effectiveness.

The electronic readout system[12] used with the tungsten wire anode plane consists of 64 channels of hybrid preamplifiers, post amplifiers, discriminators and multi-hit time to digital converters (Fig. 6a). The system was operated with 10 ns time bins and spanned 30 μsec. The carbon wire anodes were instrumented with LeCroy HQV810 preamplifiers and shapers. Both ends of the center 16 wires were read into fast waveform digitizers (Fig. 6b).

The gas system is shown schematically in Fig. 6c. It includes part-per-million oxygen and water monitors, plus UV transparency and electron drift monitoring.

RUN PARAMETERS

The data were taken with low energy tagged electron and pion beams at the SLAC Test Beam Facility under various

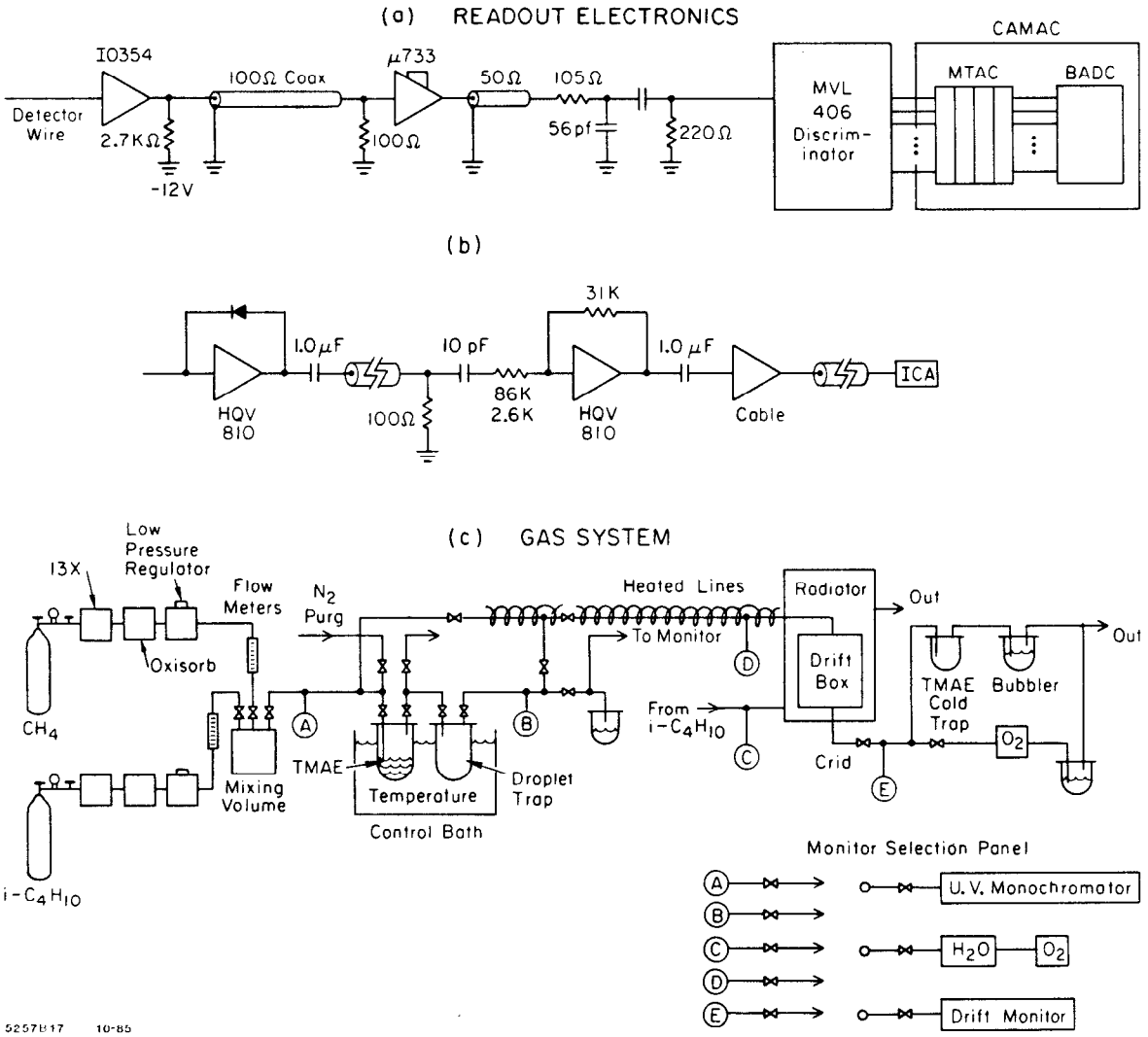

Fig. 6. a) Electronics readout system used with the single ended tungsten wire anode. b) Electronics used with carbon filaments. c) The gas system.

combinations of the parameters listed below.

• Momenta (GeV/c)	3.96	6.5	11.0	
• TMAE Temperature °C	5	19	28	
• Drift Field V/*cm*	100	200	300	400
• Detector Gas (CH_4/iC_4H_{10} %)	90/10	80/20		
• Blinding Grid	ON	OFF		
• Radiator (Gas, Liquid)	G and L	G only	L only	

THE DATA

Figure 7a is an on-line display of CRID hits for about 200 events with both radiators. The two large arcs are from the liquid ring and the small circle is the gas ring. The dark spot in the center is the beam track and its associated "photon feedback". The long tail following the beam spot is due to saturation effects in the amplifiers caused by the heavy ionization of the beam track. Figure 7b is the projection of the data on the time axis. An important additional feature is now more obvious: there is a serious electron "lifetime" problem. The

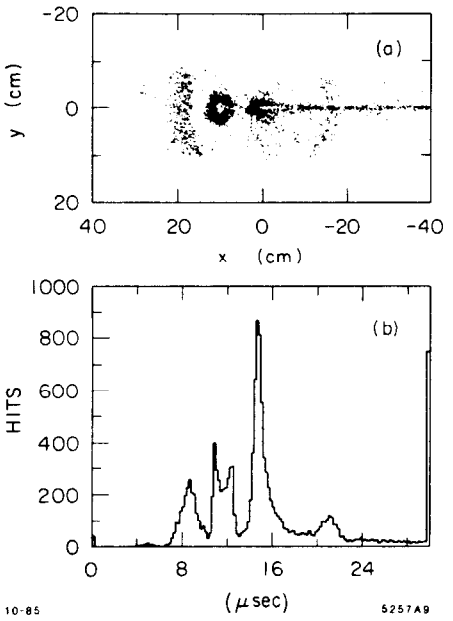

Fig. 7. a) On-line residual plot of about 200 events; y is the wire address and x is derived from the drift time; b) Projection on the time axis.

leading liquid arc (at 8 μsec) has a substantially larger number of hits than the trailing liquid arc (at 20 μsec). Assuming the two peaks are initially equally populated, the electron lifetime is given by

$$\tau = \frac{\Delta t}{ln(N_1/N_2)}$$

where N_1 and N_2 are the number of hits in the peaks (with background subtracted) and Δt is their drift time difference. For this particular run $\tau = 10$ μsec, which for a drift velocity of 4.5 cm/μsec, gives an electron absorption length of 45 cm. This is much less than the five or more meters that is desired for the SLD to keep losses over the maximum drift distance of 75 cm at a negligible level. Before introducing TMAE into the TPC, electron "lifetimes" of up to 120 μsec were measured; with TMAE the lifetime varied from $\sim$ 20 μsec down to $\sim$ 6 μsec. The lifetime was independently monitored during the run with a pulsed N_2 laser by varying the drift field voltage and hence the drift time (the detector gas is not saturated), giving consistent results.

Figure 8 shows the results of determining the electron lifetime using the mean number of observed photoelectrons in the gas ring as a function of the drift field. This particular set of data gives 6.5 μsec. This problem is believed to be due to the great chemical activity of TMAE and the extreme electronegativity of some of its reaction by-products. A substantial research program is in progress to determine the source of the electronegative components of the detector gas, to understanding how to clean and handle TMAE, and determine what materials must be avoided in the construction of the CRID drift boxes and plumbing.

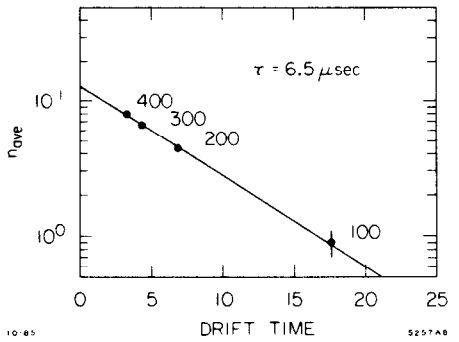

Fig. 8. The average electron "lifetime" derived from the number of electrons on a gas ring versus the electron drift time. The drift time is determined by the drift field which is shown on the figure in V/*cm*.

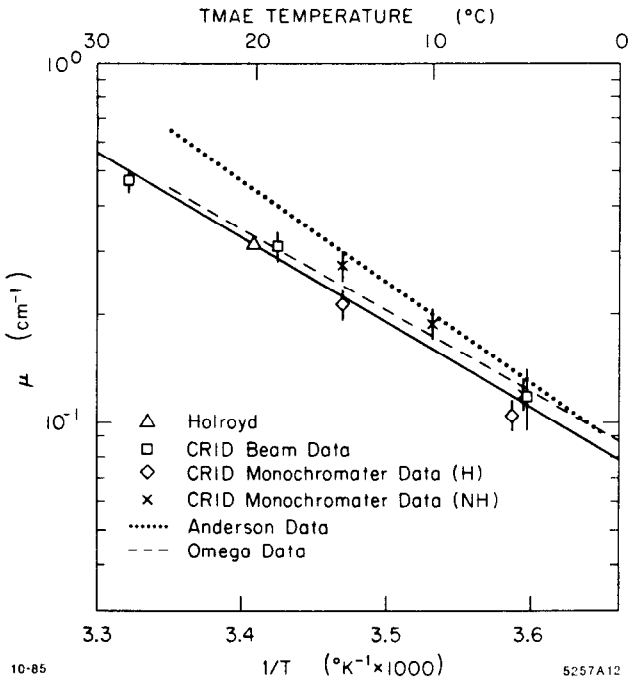

Fig. 9. TMAE absorption coefficient ($1/cm$) versus reciprocal temperature. The triangular point is a measurement by Holroyd. Data taken with TMAE purified by Holroyd are labeled "H"; other data are labeled "NH".

The TMAE sample used in these tests was purified by Richard Holroyd of Brookhaven National Laboratory.[13] The (initial) level of impurities was very low. Measurements of the absorption coefficient as a function of wavelength in the UV were made during the run using a UV monochromator. Figure 9 shows some of these measurements compared to those of Anderson,[5] the OMEGA[14] group, and a point measured by Holroyd. Also shown are direct measurements of the attenuation of Čerenkov photons in the TPC by a method described below. Our measurements of the Holroyd TMAE are consistently below (more transparent) than those of Anderson and the OMEGA group. If the longer attenuation length is due to the removal of UV absorbing impurities (which compete with photoionization), then the effective quantum efficiency of TMAE should be increased.

PHOTON FEEDBACK

Because the TPC is sensitive to single Čerenkov photons, it is also sensitive to photons generated in the avalanche process which result in a background referred to as photon feedback. The number of such feedback photons is proportional to the size of the avalanche, *i.e.*, the gain. This process is already important at the single electron level when operating at a gas gain of 1 or 2 $\times 10^5$. A minimum ionizing particle can leave a trail of several hundred electrons, so this effect must be suppressed by several orders of magnitude. As shown in Fig. 5 a combination of cathode walls and wire grids were used. The cathode structure has an opening angle into the drift volume of $\sim 90°$. With the grid in place, the angle is reduced to $\sim 14°$ giving additional reduction factor of six. Figure 10 compares data taken with and without the blinding grid, where all non-electronically generated hits between the beam spot and the fiducial arc of the liquid ring are tallied. The ratio of the means of the distributions agrees with the expected geometrical suppression factor within uncertainties of the method.

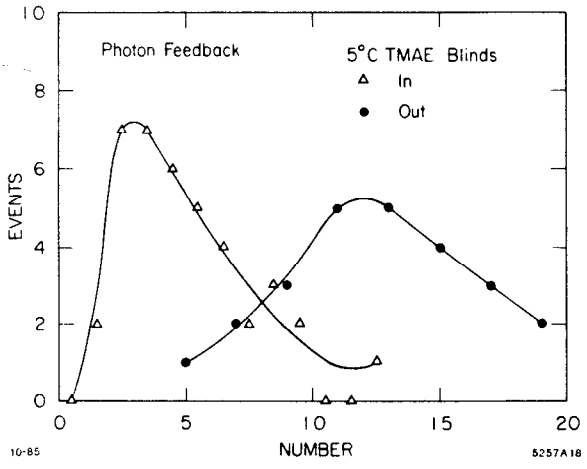

Fig. 10. Number of "photon feedback" hits per event with and without the blinding grid described in the text.

In addition, the trailing edges of gas ring data with and without the blinding grid were compared at a gain of 2×10^5. Without the blinding grid, an upper limit of approximately 35% of single avalanches produce a feedback hit.

THE LIQUID RING

Without third coordinate information the radius distribution of the liquid ring is very broad due to the steep angle of incidence and the TMAE absorption length (which at 5°C is about 10.5 *cm*). The assumption of exponential absorption in TMAE integrated over the width of the Čerenkov cone leads to the radius distribution shown in Fig. 11a.

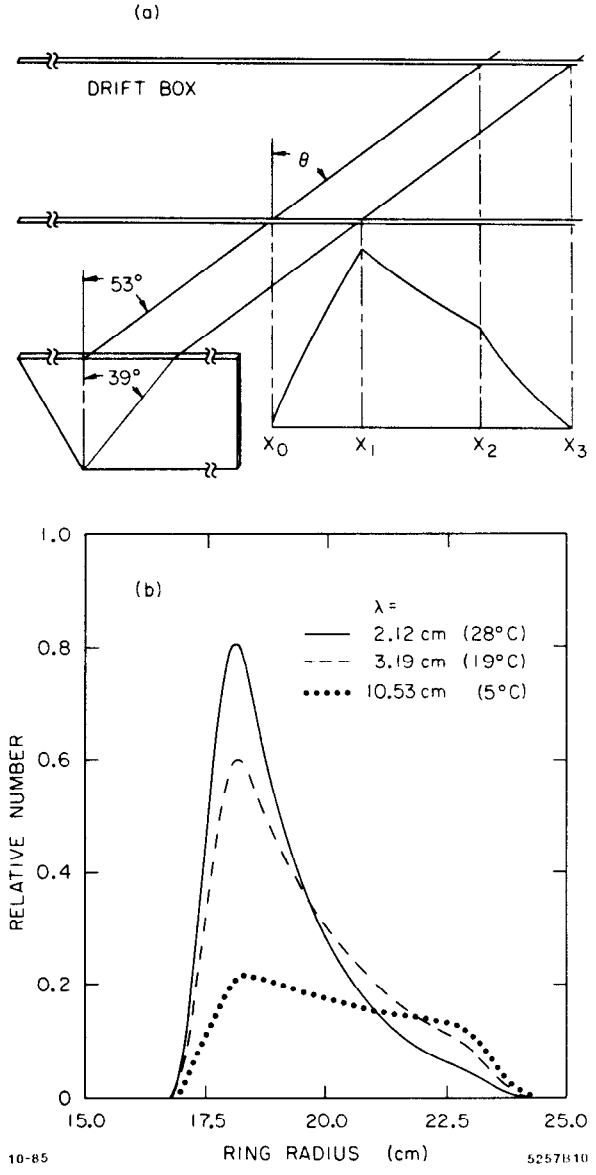

Fig. 11. a) Model of the shape of the liquid ring radius plot showing the Čerenkov photons from the C_6F_{14} radiator impinging on the TPC. Each photon is absorbed with an exponential absorption length λ, and integrating in y gives the distribution shown. The distribution rises as $1 - \exp^{-x/\lambda'}$, between x_1 and x_2 it falls as $(\exp^{x_1/\lambda'} - 1)\exp^{-x/\lambda'}$, and beyond x_2 where photons leave, it falls like $\exp^{(x_1-x)/\lambda'} - \exp^{-x_2/\lambda'}$, where $\lambda' = \lambda \sin\theta$. Fitting an exponential between x_1 and x_2 gives the TMAE absorption length. b) Monte Carlo of the liquid radius plot including chromatic dispersion for three absorption lengths.

The peak occurs where the outer radius of the ring intersects the TPC (x_1 in the figure). If the absorption length in TMAE is comparable to the path length through the box, then there will be a kink in the distribution where the photons begin to leave the other side. The region between the peak and the kink falls exponentially with a slope equal to the inverse of the (projected) TMAE absorption length. Thus we can get a direct measurement of the TMAE absorption length from this plot. A Monte Carlo calculation of the profile, including chromatic dispersion effects, for three TMAE concentrations is shown in Fig. 11b. Although this model does not fully describe the data due to other effects such as photon feedback, it does account for the basic features as shown in Fig. 12. Several measurements of the TMAE absorption length at different temperatures are shown in Fig. 9, as previously mentioned.

With the third coordinate readout, the uncertainty in Čerenkov angle for a single event will be dominated by the geometrical and chromatic errors, and is predicted to be 1.5 mr for 23 photoelectrons.

Figure 11a shows the relationship of the peak of the radius plot to the Čerenkov angle: $R_{peak} = l \tan\theta_r + d \tan\theta_c$, where l is the distance between the radiator and the TPC and d is the radiator thickness. Also $n \sin\theta_c = \sin\theta_r$ where n is the index of refraction of the liquid. Thus n and θ_c can be found simultaneously (numerically). For 11 GeV/c pions and 28° TMAE, an index of refraction of 1.280 ± 0.002 and a Čerenkov angle of 38.62° ± 0.12° are found. The refracted angle is 53.0° ± 0.3°. The index agrees well with the known value of 1.277 at 1900 Å. With the third coordinate readout, the uncertainty in Čerenkov angle for a single event will be dominated by the geometrical and chromatic errors, and is predicted to be 1.5 mrad for 23 photoelectrons. The distribution of the observed number of hits per event in the leading arc of the liquid ring is shown in Fig. 13; the mean is 3.8 ± 0.4. Since the arc is only about 68°, the full circle will be greater by a factor of 5.3, and thus have 20 hits. Taking into account the radiator length and electron absorption losses give 37 ± 5 for 1 *cm* radiator, or an N_0 of 94 ± 14/*cm*. Backgrounds due to photon feedback and random hits are estimated to be a few percent and do not account for this surprisingly large result.

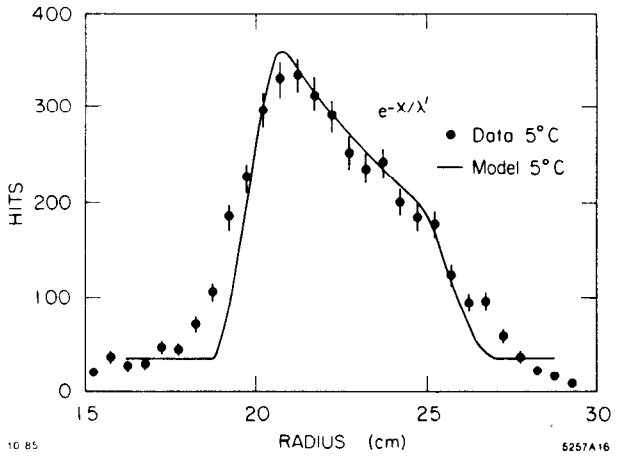

Fig. 12. Comparison for the liquid radius plot with the model for 5°C TMAE.

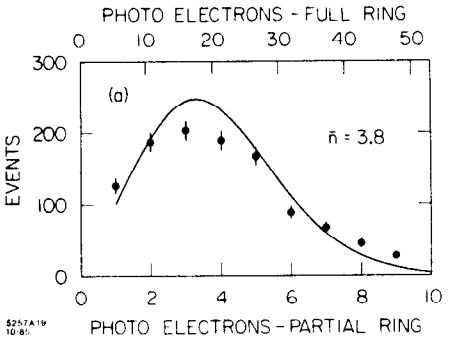

Fig. 13. The number of photoelectrons on the leading arc of the liquid ring. The upper scale gives the number on a full circle.

THE GAS RING

Figure 14a is an event averaged (with a mean number of five) radius plot of 11 GeV/c pions in the gas radiator after projecting the hits onto the focal plan of the mirror. Figure 14b shows a Monte Carlo simulation of the gas ring including the TMAE absorption length, diffusion in the drift gas, detector binning resolution and geometrical effects. This model is in excellent agreement with the data. The derived Čerenkov angle of 56.6±1.7 mrad for an 11 GeV/c pion corresponds to an index of refraction for the isobutane radiator of 1.00168±0.0001. The standard deviation of the distribution is 3.2 mrad; it is dominated for these data by depth uncertainty due to the TMAE absorption length of 2.4 *cm*.

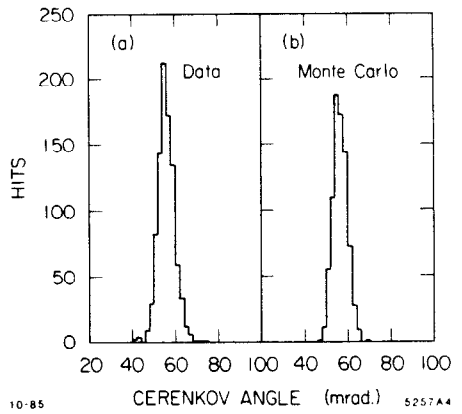

Fig. 14. The event averaged Čerenkov angle for the gas ring; a) data and b) Monte Carlo.

Figures 15a and 15b show the momentum dependence of the Čerenkov angle for tagged pions and electrons. The data have some scatter, but agree well with expectations.

Figures 16a and 16b are examples of 3.96 GeV/c tagged electron and pion events respectively. The solid lines are best fit circles, while the dotted lines are electron and pion hypotheses. There is clear event by event separation. Figure 17 shows accumulated radius plots for 3.96 GeV/c tagged electrons and pions. The separation of the peaks is 11 mrad and the widths are 4.2 and 3.3 mrad respectively giving about 2.5 σ separation.

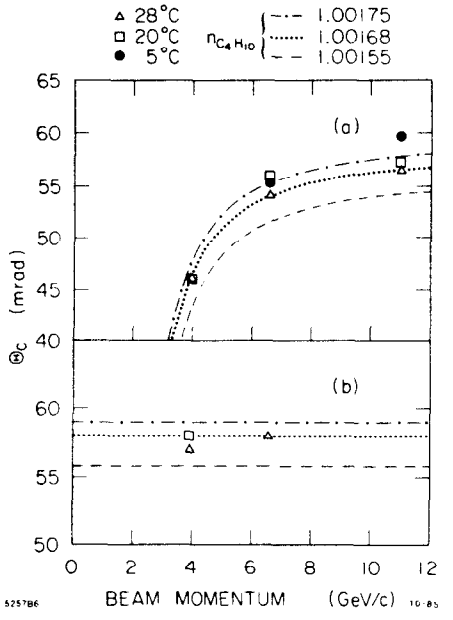

Fig. 15. The dependence of the measured Čerenkov angle for three TMAE temperatures on momentum for a) pions and b) electrons. Theoretical curves for three values of the isobutane index of refraction are shown. A value of $n = 1.00168$ is preferred.

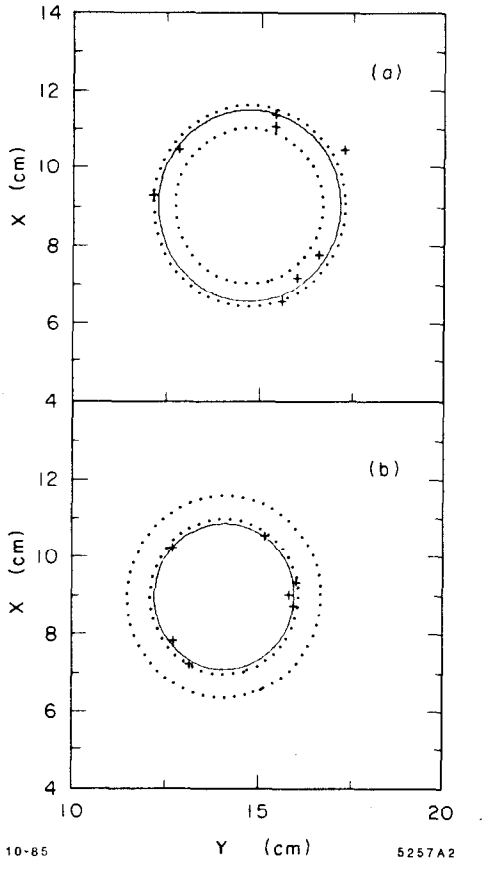

Fig. 16. Examples of typical tagged a) electron and b) pion events at 3.96 GeV/c. The solid curves are best fits to the data while the dotted circles are the two hypotheses.

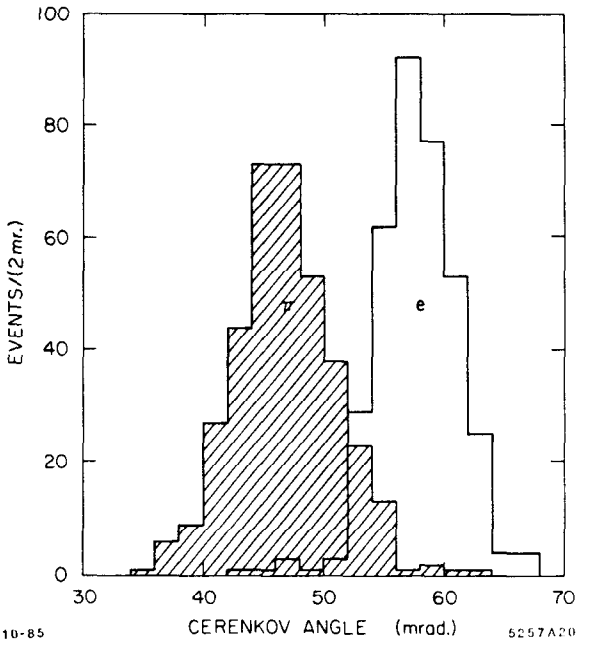

Fig. 17. The Čerenkov angles for 3.96 GeV/c tagged electrons and pions events.

Figure 18 shows the distribution of the number of hits on a gas ring for 11 GeV/c pions. The ring is positioned near the top of the drift box to minimize lifetime losses. The data are well fit by a Poisson distribution of mean 7. This run has a measured lifetime of 6.5 μsec; extrapolation to zero drift time gives a yield of 13 ± 0.5 photoelectrons per event, giving an N_0 of $90 \pm 4/cm$, in good agreement with the SLD Design Report.[3]

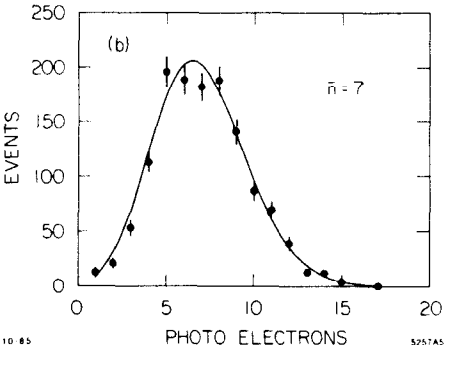

Fig. 18. The number of gas ring hits per event for 28°C TMAE.

THIRD COORDINATE

A carbon filament anode plane was installed at the very end of the data run, and a small amount of data taken with both liquid and gas radiators. The analysis of this data is still preliminary, and work on it is continuing. Figure 19 compares the radius plot for the liquid ring with and without the use of the charge division information. The standard deviation has decreased by almost a factor of three, to $0.83° \pm 0.006°$ per photoelectron which is quite close to the expected value of $\sim 0.73°$ based on known systematic errors in this data. An ultimate

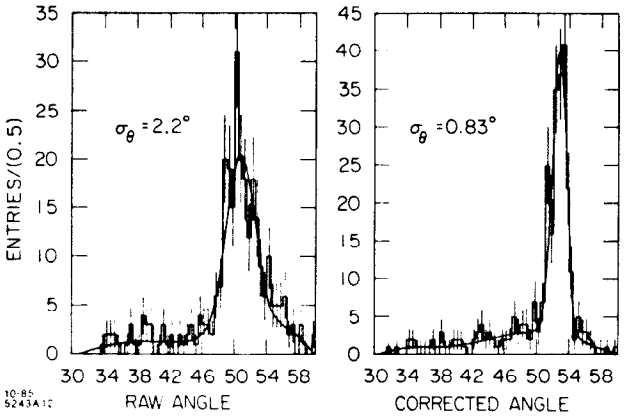

Fig. 19. The Čerenkov angle a) without charge division and b) with charge division using a carbon filament anode plane.

resolution for the liquid ring of $\sim$ 0.5° per photoelectron is expected.

SUMMARY AND ACKNOWLEDGEMENTS

In summary, we have operated a full scale demonstration CRID incorporating most of the essential features of the SLD CRID design. The measured values of N_0 of 90 for both the liquid and gas radiators are equal to or greater than the SLD specifications. The resolution, without third coordinate readout is in excellent agreement with expectations: We have observed e/π separation of 2.5 σ at 4 GeV/c and measured Čerenkov angles in excellent agreement with the known values of refractive indices of the radiators. We have demonstrated substantial suppression of photon feedback while maintaining full efficiency. We have built and begun testing a carbon wire charge division detector for third coordinate readout. Preliminary results indicate that the system is robust and will give the desired performance.

The excellent technical support of T. Weber and H. Peterson is gratefully acknowledged.

REFERENCES

1. S. Williams, et al., IEEE Trans. Nucl. Sci. NS-32, 681, (1985).
2. S. Williams, "Čerenkov Ring Imaging Detector Development at SLAC," SLAC-PUB-3360, (1984).
3. M. Breidenbach, et al., "The SLAC Linear Collider Detector," these Proceedings and SLD Design Report SLAC-273.
4. Seguinot, J., and Ypsilantis, T., Nucl. Inst. and Meth. 142, 377 (1977).
5. Anderson, D.F., IEEE Trans. Nucl. Sci. NS-28, 842, (1981).
6. For safety reasons, we are also studying the use of perfluoropentane, C_5F_{12}, which has a slightly better (higher) index of refraction and is somewhat more transparent, but is expensive and has a boiling point of 29°C. The liquid radiator material is the related compound perfluorohexane, C_6F_{14}. These compounds are manufactured by 3M Corporation, St. Paul, Minnesota (FC-88 and FC-72), and by ISC Chemicals, Great Britain (PP-50 and PP-1).
7. Acton Research Corp. Acton, Massachusetts.
8. Oxisorb is a trace oxygen and water removal filter manufactured by Schweisstechnik, AG, Zurich, Switzerland.
9. Hereaus & Co., Federal Republic of Germany.
10. On loan from the RICH group at Rutherford Laboratory, Great Britain
11. F. Bird, et al., "Charge Division Using Carbon Filaments for Obtaining Coordinate Information from the Detection of Single Electrons," these Proceedings.
12. The IO354 hybrid preamplifiers were obtained from V. Radaka at Brookhaven National Lab. The MVL406, HQV810, and the 2242 Image Chamber Analyzer (ICA) are products of LeCroy Research Systems Corp., Spring Valley, N.Y.
13. R. Holroyd, Brookhaven National Laboratory, private communication.
14. R. J. Apsimon, et al., RAL 85-014 (submitted to NIM).